Electronic Supplementary Material (ESI) for Chemical Communications.

Electronic Supplementary Information

Ordered Alignment of a One-Dimensional π-Conjugated Nickel Bis(dithiolene) Complex Polymer Produced *via* Interfacial Reactions

Ryota Matsuoka, Ryota Sakamoto,* Tetsuya Kambe, Kenji Takada,
Tetsuro Kusamoto, and Hiroshi Nishihara*

Department of Chemistry, Graduate School of Science, The University of
Tokyo, 7-3-1 Hongo, Bunkyo-ku, Tokyo 113-0033, Japan

Contents

A. Methods

Materials. $Ni(OAc)_2{\cdot}4H_2O$ and acetonitrile (HPLC grade) were purchased from Kanto Chemical Co., Inc. NaBr was received from Wako Pure Chemical Industries, Ltd. Dichloromethane was purified with a Glass Coutour Solvent Dispensing System (Nikko Hansen & Co., Ltd.). Water was purified using the Milli-Q purification system (Merck KGaA). Benzenetetrathiol (BTT)[1a] and NaTCNQ[1b] were synthesised according to the method described previously. HOPG was purchased from Alliance Biosystems, Inc. (Grade SPI-1 10 × 10 × 2 mm) and cleaved with adhesive tape just before use. Natural mica plates were purchased from Nilaco Corporation. They were cut in 2 cm × 2 cm, and cleaved with pieces of adhesive tape prior to use.

Preparation of 1. Under an argon atmosphere, 1.0 mg of BTT was added to degassed dichloromethane (10 mL) in a cylindrical glassware with a diameter of 40 mm, to prepare a solution with a concentration of 0.48 mM. The dichloromethane solution was then covered with degassed pure water (10 mL) to form an oil-water double layer. A degassed aqueous solution (10 mL) containing $Ni(OAc)_2$ (50 mM) and NaBr (10 mM) was carefully added to the water phase. After waiting for 1 day, **1** emerged at the interface as a thin dark brown film. After emerging the thin film of **1** at the oil-water interface, the aqueous layer was replaced with pure water, and **1** was deposited on HOPG by means of the Langmuir-Blodgett (LB) method[2]. For the electrochemical measurement, **1** suspended in ethanol was casted dropwise on HOPG. The drop casting was repeated five times in order to increase the current signal.

Chemical reduction of 1. Under an Ar atmosphere, several flakes of the film of **1** (ca. 3 mm × 3 mm) was added to a degassed solution of NaTCNQ (0.33 mg) in acetonitrile (10 mL). The solution was refluxed for 19 h. Resultant reduced **1** was picked up using a pipette, and washed with degassed acetonitrile. Reduced **1** was then casted dropwise on HOPG, dried in vacuo, and subjected to an XPS measurement.

Characterisation. FE-SEM images were collected using JEOL JSM-7400FNT (JEOL EX-2300). TEM images were recorded at 75 kV using Hitachi HF-2000 equipped with an AMT-CCD camera. The TEM samples were prepared by depositing **1** on a copper grid, using ethanol suspension of **1**. IR-ATR spectra were recorded using Jasco FT/IR-6100 at room temperature under vacuum. XPS data were obtained using PHI 5000 VersaProbe (ULVAC-PHI, INC.). Al Kα (15 kV, 25 W) was used as the X-ray source, and the beam was focused on a 100-μm^2 area. The spectra were analyzed using MultiPak Software, and standardised using the C(1s) peak at 284.6 eV. SPM measurement was carried out using Agilent Technologies 5500 Scanning Probe Microscope, under an ambient condition. AFM was performed in the high-amplitude mode (trapping mode), with silicon cantilever PPP-NCL (Nano World). Probes for STM were cut from a wire (Pt-Ir alloy, 4:1, 0.25 mmϕ) using a nipper, to obtain a sharp tip. Electrochemical measurements were recorded using ALS 650DT electrochemical analyzer (BAS. Co., Ltd.). A homemade Ag^+/Ag reference electrode (0.01 M $AgClO_4$ in 0.1 M Bu_4NClO_4/acetonitrile) and a Pt wire counter electrode were implemented in order to establish a three-electrode system. Bu_4NClO_4, acting as a supporting electrolyte, was recrystallised from EtOH and put under vacuum for 24 h. Ferrocene was used as an internal standard.

Electrical property. The electrical conductivity of as-prepared **1** was measured using a preliminary two-electrode configuration. Two pieces of Cu tape as the electrode were attached to a small flake of **1** on mica using a eutectic alloy of gallium and indium as a conductive glue. A typical size of **1** was 1.2 mm and 0.87 mm in width and depth (measured using a digital microscope supplied by Keyence corporation, the width corresponds to the distance between the electrodes), and 0.70 μm in height (from AFM cross-section analysis). I–V data was collected using ALS 650DT electrochemical analyzer.

B. Deconvolution of the S 2s peaks in the XPS of **1**

(a)

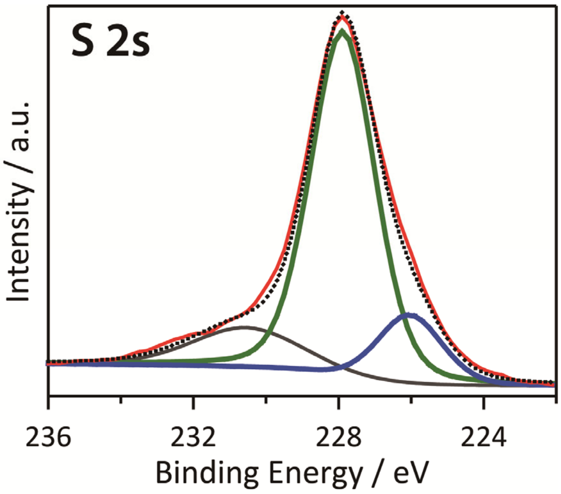

(b)

Band	Binding energy / eV	FWHM / eV	Area / %
1	230.5	3.54	14.0
2	227.9	2.10	71.7
3	226.1	2.10	14.3

Fig. S1 (a)Deconvolution of the S 2s peak. The green and blue Gaussian curves are derived from the nickel bis(dithiolene) moieties in the 0 and -1 oxidation states, respectively. On the other hand, the grey one is assigned to the "shake-up" peak.[3] The red line is the experimental S 2s peak, whereas the dotted black line corresponds to the sum of the Gauss curves (i.e. simulated spectrum). (b) Information on the Gaussian curves. The average oxidation number of the nickel bisdithiolene unit is −0.17, with a ratio of 5:1 for the 0 and −1 oxidation states.

C. XPS of reduced **1** and deconvolution of the S2s peak

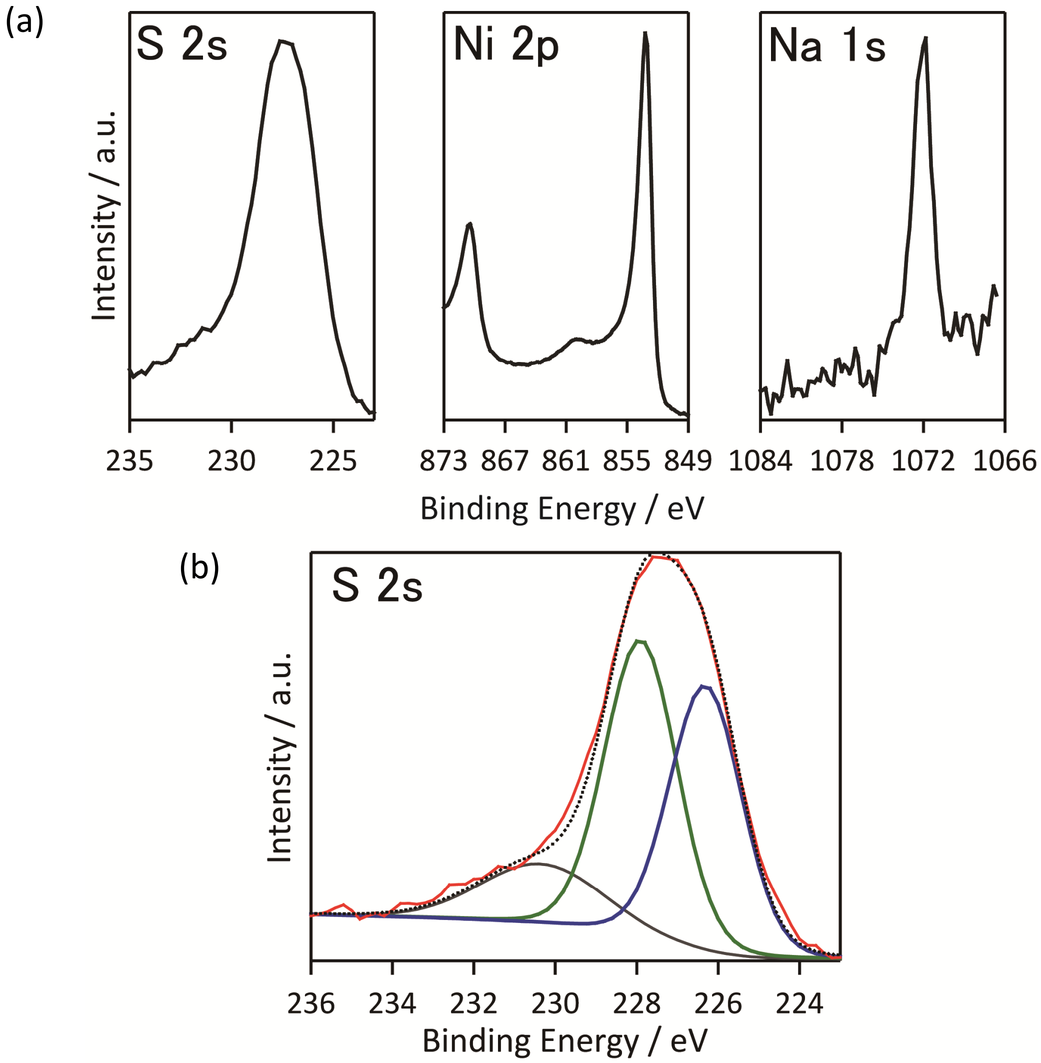

(c)

Band	Binding energy / eV	FWHM / eV	Area / %
1	230.3	3.54	14.8
2	227.9	2.10	44.8
3	226.3	2.10	40.4

Fig. S2 (a) XPS of reduced **1** focusing on the S 2s, Ni 2p, and Na 1s regions. (b)Deconvolution of the S 2s peak. The green and blue Gaussian curves are derived from the nickel bis(dithiolene) unit in the 0 and -1 oxidation states, respectively. On the other hand, the grey one is assigned to the "shake-up" peak.[3] The red line is the experimental S 2s peak, whereas the dotted black line corresponds to the sum of the Gaussian curves (i.e. simulated spectrum). (c) Information on the Gaussian curves. The average oxidation number of the nickel bisdithiolene unit is −0.47, with a ratio of 1.1:1 for the 0 and −1 oxidation states. This value is less than that of as-prepared **1**, thus the reduction proceeded partially. Judging from the redox potentials of **1** (0.20 V vs Fc^+/Fc) and NaTCNQ (−0.30 V vs Fc^+/Fc), **1** should be reduced into the −1 monovalent state. The incomplete reduction probably stems from re-oxidation through oxygen contamination: The authors conducted the chemical reduction under an inert atmosphere, but reduced **1** was subjected to air for a short time when it was casted onto HOPG, and was transferred to the XPS apparatus.

D. Computational Study

In order to estimate the nickel-nickel distance of **1**, DFT calculation for tetranuclear nickelladithiolene complex **2** (Fig. S3) was carried out. The Gausian 09 program[4] was used for the geometrical optimisation of **2**. The structure was optimised without any symmetry constraint. To simplify the calculation, the oxidation state of **2** was fixed to 0 with a singlet ground state. The B3LYP hybrid exchange-correlation functional[5] was employed. The LanL2DZ basis set[6] was used for the Ni atoms, and the 6-31G(d) basis set[7] for the other atoms. Visualisation of the result was performed using GaussView 5.0.8 software[8].

Optimised **2** has a totally planer structure. The nearest Ni—Ni distance is 0.8507 nm and 0.8513 nm for the outside pair and the inside pair, respectively. Hence, the nearest Ni-Ni distance in coordination polymer **1** is estimated to be 0.85 nm.

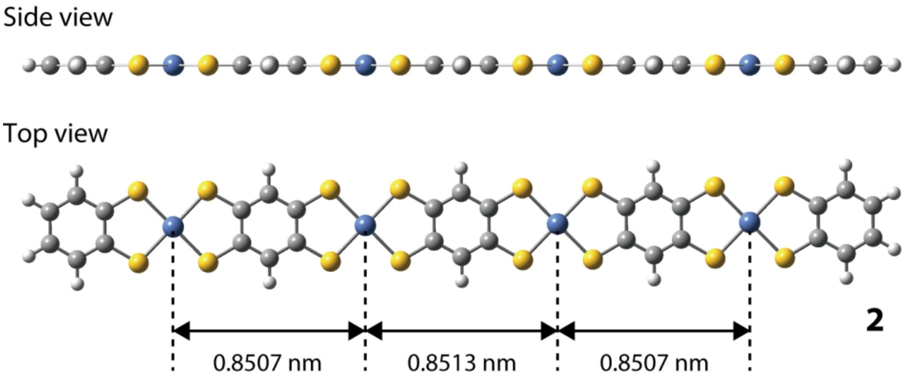

2

Fig. S3 Optimised structure of **2**. Grey, C; White, H; yellow, S; blue, Ni.

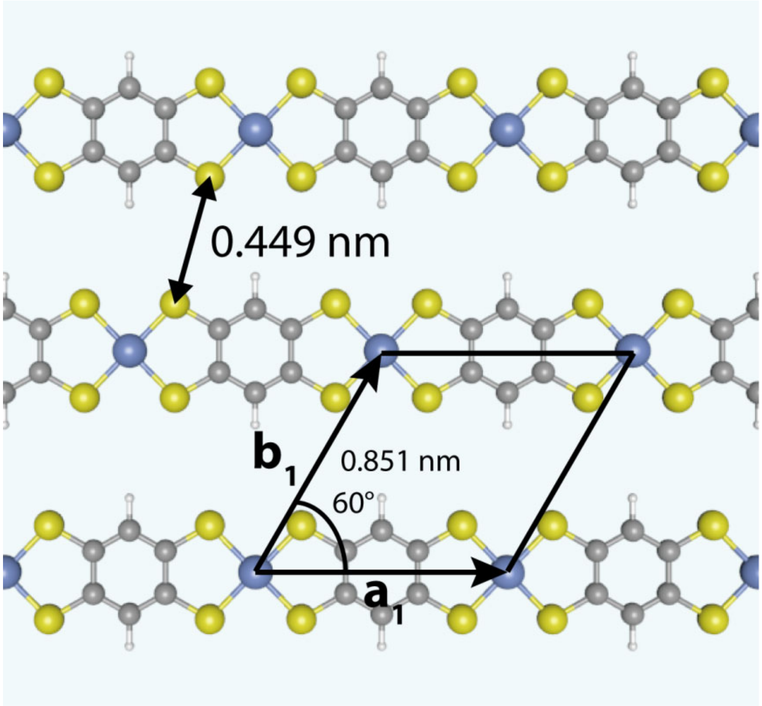

Fig. S4 Pseudo-hexagonal lattice composed of **1** aligned in an A-B-A fashion. The distance between the two nearest S atoms of two neighboring wires is calculated to be 0.449 nm, which is comparable to those of one-dimensional nickel bis(dithiolene) coordination polymers in the solid state deduced from LAXS and EXAFS analysis.[9]

E. Analysis of the moiré structure of **1** on HOPG

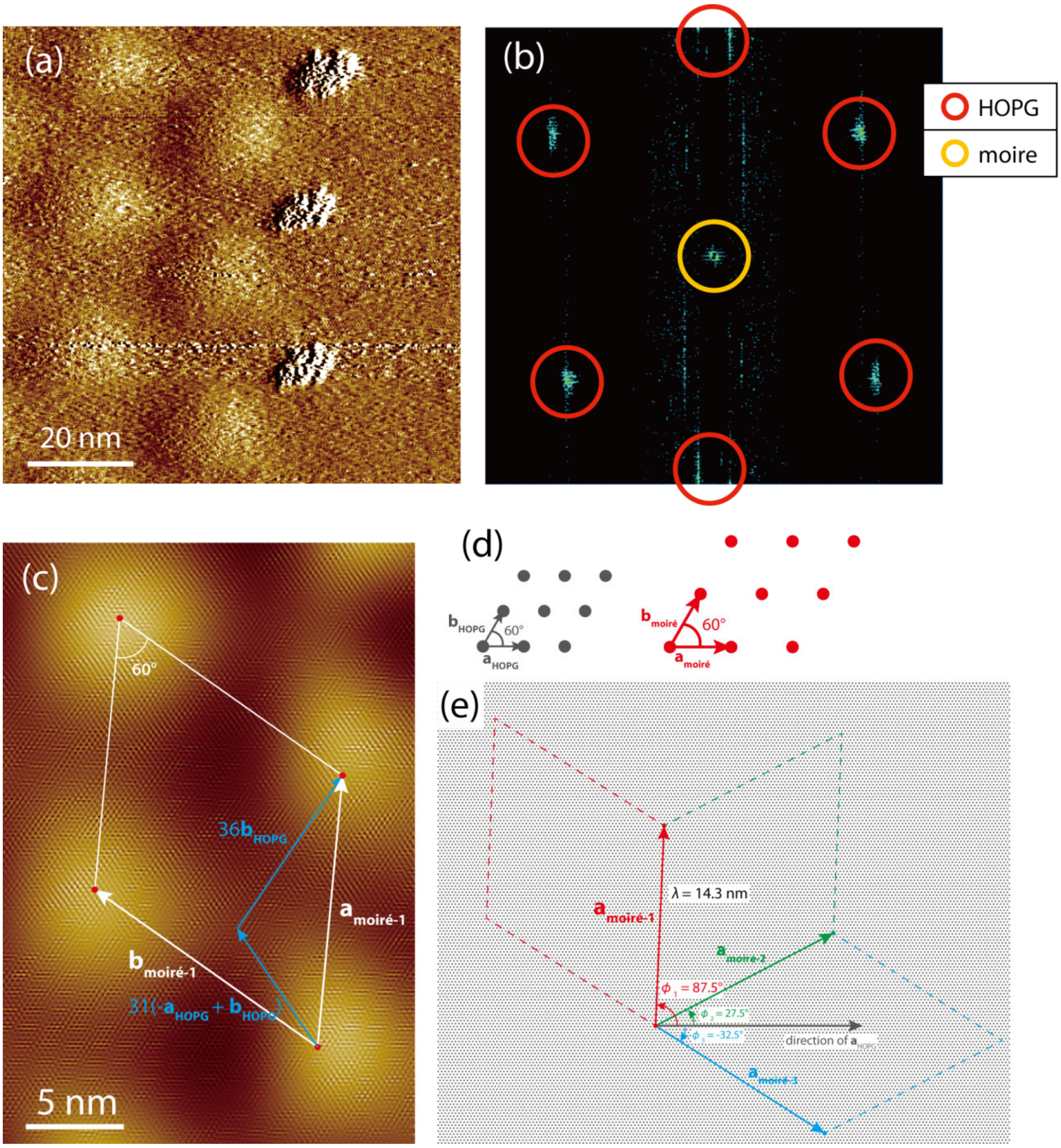

Fig. S5 (a) Observed moiré interference structure derived from monolayer of **1** and HOPG. (b) FFT image of (a). (c) Moiré structure highlighted by inverse FFT. The greater lattice is the moiré pattern, whereas the smaller one stems from the direct structure of HOPG. (d) Lattice vectors of HOPG and monolayer of **1**. (e) Simplified model of the HOPG and moiré lattices.

The moiré and HOPG lattices can be highlighted from the STM image by means of inverse FFT (Fig. S5a-c). The HOPG hexagonal lattice is known ($|\mathbf{a}_{\mathrm{HOPG}}| = |\mathbf{b}_{\mathrm{HOPG}}| = 0.246$ nm, where $\mathbf{a}_{\mathrm{HOPG}}$ and $\mathbf{b}_{\mathrm{HOPG}}$ are the unit vectors of the HOPG lattice, Fig. S5d). Then we first determine the lattice length of the moiré pattern λ ($= |\mathbf{a}_{\mathrm{moiré}}| = |\mathbf{b}_{\mathrm{moiré}}|$, where $\mathbf{a}_{\mathrm{moiré}}$ and $\mathbf{b}_{\mathrm{moiré}}$ are the lattice vectors of the moiré pattern, Fig. S5c,d), and the rotation angle of the moiré lattice ϕ with respect to the HOPG lattice (= the rotation angle of $\mathbf{a}_{\mathrm{moiré}}$ with respect to $\mathbf{a}_{\mathrm{HOPG}}$, Fig. S5e, the counterclockwise direction is defined as positive).

Due to the six-fold symmetry of the moiré and HOPG lattices, we have to consider three ϕ, -32.5°, 27.5°, and 87.5°, which are derived from three $\mathbf{a}_{\mathrm{moiré}}$, $\mathbf{a}_{\mathrm{moiré\text{-}1}}$, $\mathbf{a}_{\mathrm{moiré\text{-}2}}$, and $\mathbf{a}_{\mathrm{moiré\text{-}3}}$ (Fig. S5e). These unit vectors are represented as eqs. (S1), (S2) and (S3), respectively:

$$\mathbf{a}_{\mathrm{moiré}-1} = 36\mathbf{b}_{\mathrm{HOPG}} + 31(-\mathbf{a}_{\mathrm{HOPG}} + \mathbf{b}_{\mathrm{HOPG}}) \tag{S1}$$

$$\mathbf{a}_{\mathrm{moiré}-2} = 36\mathbf{a}_{\mathrm{HOPG}} + 31\mathbf{b}_{\mathrm{HOPG}} \tag{S2}$$

$$\mathbf{a}_{\mathrm{moiré}-3} = 36(\mathbf{a}_{\mathrm{HOPG}} - \mathbf{b}_{\mathrm{HOPG}}) + 31\mathbf{a}_{\mathrm{HOPG}} \tag{S3}$$

Therefore, all cases give λ of 14.3 nm.

The in-plane lattice constant of HOPG ($|\mathbf{a}_{\mathrm{HOPG}}| = |\mathbf{b}_{\mathrm{HOPG}}| = 0.246$ nm) is much smaller than that of the monolayer of **1** ($|\mathbf{a}_1| = |\mathbf{b}_1| \sim 0.85$ nm, where $\mathbf{a}_1$ and $\mathbf{b}_1$ are the unit vectors of the monolayer of **1**, Fig. S3 and S4). The size mismatch between the two lattices is too large to form the observed moiré pattern. Then we propose three linear combinations of $\mathbf{a}_{\mathrm{HOPG}}$ and $\mathbf{b}_{\mathrm{HOPG}}$ with integral coefficients, which may produce the observed moiré pattern:

$$\mathbf{a}_{\mathrm{HOPG-L}} = m\mathbf{a}_{\mathrm{HOPG}} + n\mathbf{b}_{\mathrm{HOPG}} \tag{S4}$$

$$\mathbf{b}_{\mathrm{HOPG-L}} = m\mathbf{b}_{\mathrm{HOPG}} + n(-\mathbf{a}_{\mathrm{HOPG}} + \mathbf{b}_{\mathrm{HOPG}}) \tag{S5}$$

$$|\mathbf{a}_{\mathrm{HOPG-L}}| = |\mathbf{b}_{\mathrm{HOPG-L}}| = |\mathbf{a}_{\mathrm{HOPG}}| \times \sqrt{m^2 + n^2 + mn} \tag{S6}$$

where possible combinations of *m* and *n* are as follows: [*m*, *n*] = [2, 2] ($|\mathbf{a}_{\mathbf{HOPG\text{-}L}}| = |\mathbf{b}_{\mathbf{HOPG\text{-}L}}|$ = 0.852 nm), [3, 1] (0.887 nm), and [3, 0] (0.738 nm).

λ and ϕ (-90° < ϕ <90°) are given by eqs. (S7) and (S8):[10]

$$\lambda = \frac{|\mathbf{a}_{\mathbf{HOPG}}|}{\sqrt{2(1+\delta)(1-\cos\theta)+\delta^2}} \quad \text{when} \quad |\mathbf{a}_{\mathbf{HOPG-L}}| > |\mathbf{a}_{\mathbf{1}}|$$

$$= \frac{(1+\delta)|\mathbf{a}_{\mathbf{HOPG}}|}{\sqrt{2(1+\delta)(1-\cos\theta)+\delta^2}} \quad \text{when} \quad |\mathbf{a}_{\mathbf{1}}| > |\mathbf{a}_{\mathbf{HOPG-L}}| \qquad \text{(S7)}$$

$$\phi = \tan^{-1}\left(\frac{\sin\theta}{(1+\delta)-\cos\theta}\right) - \theta \quad \text{when} \quad |\mathbf{a}_{\mathbf{HOPG-L}}| > |\mathbf{a}_{\mathbf{1}}|$$

$$= \tan^{-1}\left(\frac{-\sin\theta}{(1+\delta)-\cos\theta}\right) \quad \text{when} \quad |\mathbf{a}_{\mathbf{1}}| > |\mathbf{a}_{\mathbf{HOPG-L}}| \qquad \text{(S8)}$$

where δ is the relative mismatch between the two hexagonal lattices:

$$\delta = \frac{|\mathbf{a}_{\mathbf{HOPG-L}}|}{|\mathbf{a}_{\mathbf{1}}|} - 1 \quad \text{when} \quad |\mathbf{a}_{\mathbf{HOPG-L}}| > |\mathbf{a}_{\mathbf{1}}|$$

$$= \frac{|\mathbf{a}_{\mathbf{1}}|}{|\mathbf{a}_{\mathbf{HOPG-L}}|} - 1 \quad \text{when} \quad |\mathbf{a}_{\mathbf{1}}| > |\mathbf{a}_{\mathbf{HOPG-L}}| \qquad \text{(S9)}$$

θ (-30° < θ <30°) is the rotation angle of $\mathbf{a}_1$ with respect to $\mathbf{a}_{\mathbf{HOPG\text{-}L}}$.

We may estimate the maximum length of the moiré pattern $\lambda_{\max}$ using eq. (S7). According to the equation, λ reaches the maximum value when θ = 0°, hence $\lambda_{\max}$ is given by eq. (S10):

$$\lambda_{\max} = \frac{1}{\delta} \times |\mathbf{a}_{\mathbf{HOPG}}| \quad \text{when} \quad |\mathbf{a}_{\mathbf{HOPG-L}}| > |\mathbf{a}_{\mathbf{1}}|$$

$$= \frac{1+\delta}{\delta} \times |\mathbf{a}_{\mathbf{HOPG}}| \quad \text{when} \quad |\mathbf{a}_{\mathbf{1}}| > |\mathbf{a}_{\mathbf{HOPG-L}}| \qquad \text{(S10)}$$

When $\lambda_{\max}$ = 14.3 nm, δ is calculated to be 0.0172 (1.72%) and 0.0175 (1.75%) by eq. (S10), respectively. Therefore, the relative mismatch between two lattices ($\mathbf{a}_{\mathbf{HOPG\text{-}L}}$ and $\mathbf{a}_1$) must be within at least 1.75% in order to make a moiré superlattice with a periodicity of 14.3 nm.

Table S1 assembles possible ranges of $|\mathbf{a}_1|$ which can make a moiré pattern with a periodicity of 14.3 nm with $\mathbf{a}_{\mathbf{HOPG\text{-}L}}$. $|\mathbf{a}_1|$ is estimated to be ca. 0.85 nm from DFT calculation (Fig. S3). Hence, all lattice vectors of HOPG cannot make a moiré lattice extending to 14.3 nm with **1**, with the exception of the case of $m = n = 2$.

Table S1. Possible ranges of $|\mathbf{a}_1|$ which can make a moiré pattern with a periodicity of 14.3 nm

lattice vector of HOPG (length of lattice vector)	Range of $|\mathbf{a}_1|$ / nm
m, n = [2, 2] (0.852 nm)	$0.838 < |\mathbf{a}_1| < 0.867$
m, n = [3, 1] (0.887 nm)	$0.872 < |\mathbf{a}_1| < 0.902$
m, n = [3, 0] (0.738 nm)	$0.726 < |\mathbf{a}_1| < 0.751$

Then we estimate the lattice constant $|\mathbf{a}_1|$ (= $|\mathbf{a}_2|$) and rotation angle θ. When $|\mathbf{a}_{\mathbf{HOPG\text{-}L}}| > |\mathbf{a}_1|$, δ and θ are given by eqs. (S11) and (S12), which are derived from eqs. (S7) and (S8):

$$\delta = \frac{1-x^2}{\sqrt{1+x^2-2x\cos\phi}} - 1 \tag{S11}$$

$$\theta = \tan^{-1}\left(\frac{x\sin\phi}{1-x\cos\phi}\right) \tag{S12}$$

where $x = \frac{|\mathbf{a}_{\mathbf{HOPG}}|}{\lambda}$

On the other hand, when $|\mathbf{a}_1| > |\mathbf{a}_{\mathbf{HOPG\text{-}L}}|$, δ and θ are given by eqs. (S13) and (S14):

$$\delta = \frac{1}{\sqrt{1+x^2-2x\cos\phi}} - 1 \tag{S13}$$

$$\theta = -\tan^{-1}\left(\frac{x\sin\phi}{1-x\cos\phi}\right) \tag{S14}$$

Experimental result gives three possible sets of parameters [λ, ϕ] at [14.3 nm, 87.5°], [14.3 nm, 27.5°], and [14.3 nm, -32.5°]. Each [λ, ϕ] gives two sets of solution [δ, θ] by eqs. (S11, S12) and (S13, S14). Hence, we obtain six sets of [δ, θ] which satisfy the experimental result. Table S2 lists the possible sets of $|\mathbf{a_1}|$ and θ', which represents an angle between $\mathbf{a_1}$ and $\mathbf{a_{HOPG}}$, giving the observed moiré pattern. δ was converted into $|\mathbf{a_1}|$ by eq. (S9), and θ was converted into θ', the rotation angle of the monolayer of **1** with respect to the HOPG lattice (Fig. S6a,b), by eq. (S15):

$$\theta' = \theta + 30° \tag{S15}$$

The DFT calculation shows that the nearest Ni—Ni distance in **1** is 0.85 nm (Fig. S3). Therefore, judging from the periodicity of monolayer of **1**, [$|\mathbf{a_1}|$, θ'] = [0.852 nm, 31.0°] and [0.853 nm, 29.0°] are the most probable pairs which can form the observed moiré pattern.

Table S2. Possible sets of $|\mathbf{a_1}|$ and θ' which give the observed moiré pattern. The blues ones are consistent with the result of DFT calculation (Fig. S3)

.

ϕ / °	-32.5	-32.5	27.5	27.5	87.5	87.5
θ' / °	30.5	29.5	30.5	29.5	31.0	29.0
$|\mathbf{a_1}|$ / nm	0.865	0.840	0.839	0.865	0.852	0.853

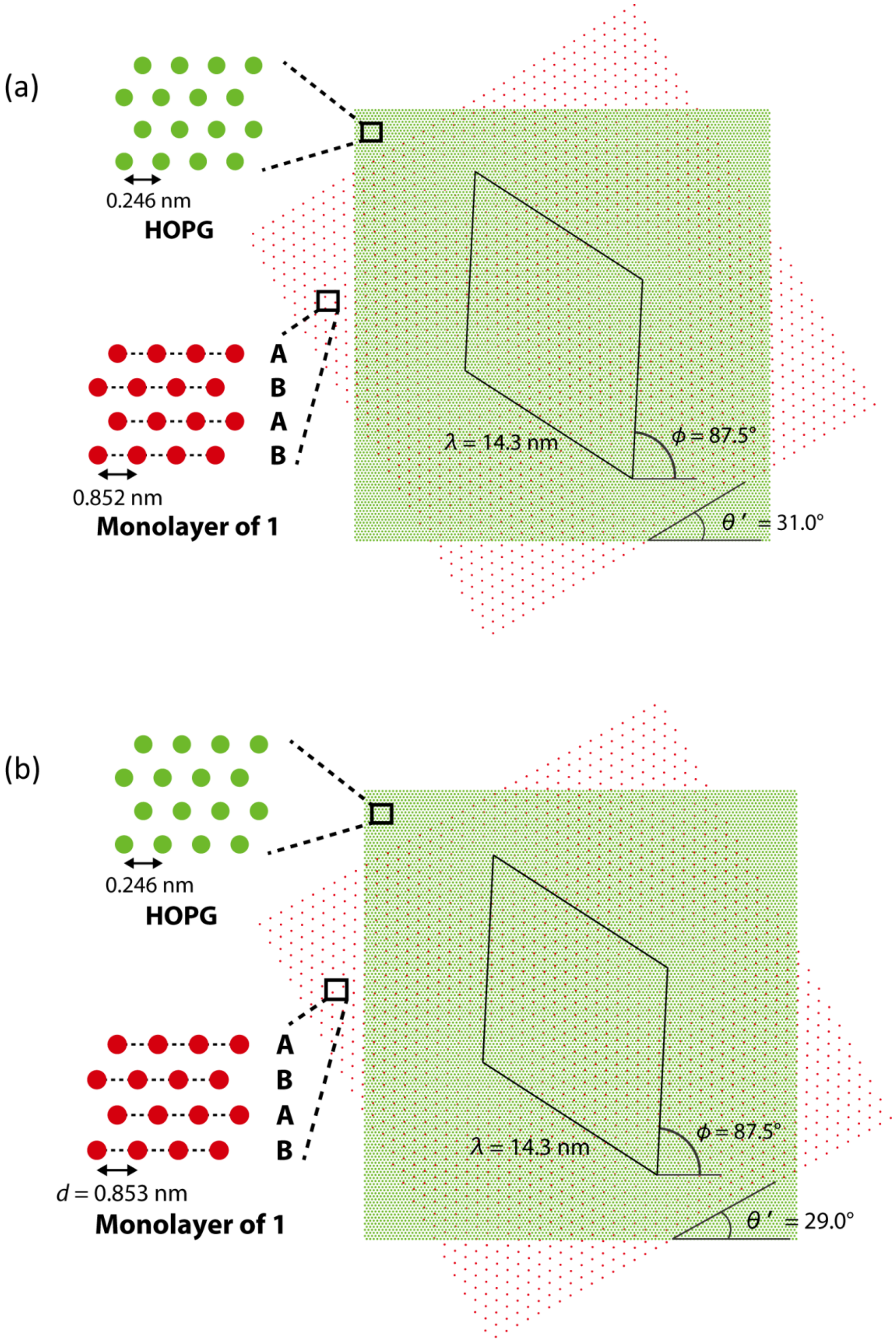

Fig. S6 Schematic illustration about the moiré pattern composed of a monolayer of **1** and HOPG substrate when (a) [$|\mathbf{a}_1|$, θ'] = [0.852 nm, 31.0°] and (b) [0.853 nm, 29.0°].

F. Gas-liquid interfacial synthesis

To investigate another way to obtain an ordered structure of **1**, a gas-liquid interfacial synthesis, which is also used to prepare the two-dimensional nickel bis(dithiolene) nanosheet,[12] was carried out. A diluted ether solution (216 μM) of BTT (3.0 μL) was gently sparged onto an aqueous solution of $Ni(OAc)_2$ (50 mM) and NaBr (10 mM) using a microsyringe. The amount of BTT was restricted such that a monolayer of BTT covered only half of the aqueous surface. The reaction system is left to stand for 2 h in an Ar atmosphere. After a spontaneous evaporation of the ether, the resultant ultrathin layer of **1** (denoted as **1′**) was then transferred on an HOPG substrate by means of the Langmuir-Schaefer (LS) method[11].

Fig. S6 shows STM height images of **1′** deposited on HOPG. The images show a striped pattern with a periodicity of 7.0 nm. The pattern has directional anisotropy. It is therefore assignable to **1′** aligned in a parallel manner with each other on HOPG. The periodicity greater than the molecular modelling (Fig. S3, 0.85 nm) is probably due to interaction between the underlying HOPG substrate.

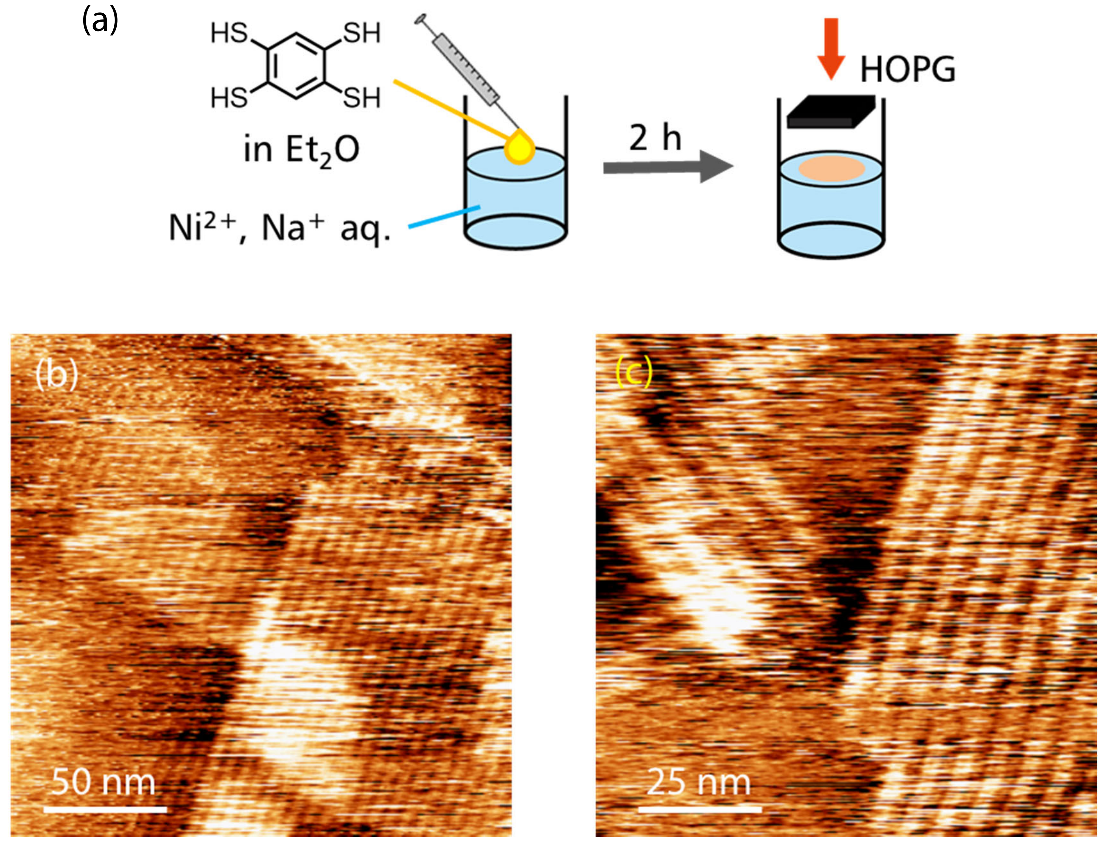

Fig. S7 (a) Schematic illustration of a gas-liquid interfacial synthesis. (b), (c) STM height images of **1** on HOPG synthesised by means of the gas-liquid synthesis. Tip bias (V_{tip}) = -700 mV; average tunnelling current (I_{t}) = 30 pA.

G. References for ESI

(1) (a) C. W. Dirk, S. D. Cox, D. E. Wellman, F. Wudl, *J. Org. Chem.* 1985, **50**, 2395. (b) L. R. Melby, R. J. Harder, W. R. Hertler, W. Mahler, R. E. Benson, W. E. Mochel, *Am. Chem. Soc.* 1962, **84**, 3374.

(2) K. B. Blodgett, I. Langmuir, *Phys. Rev.* 1937, **51**, 964.

(3) (a) S. Zhou, K. Ichimura, H. Inokuchi, *J. Mater. Chem.* 1995, **5**, 1725. (b) S.-G. Liu, Y.-Q. Liu, D.-B. Zhu, *Synth. Met.* 1997, **89**, 187.

(4) M. J. Frisch, G. W. Trucks, H. B. Schlegel, G. E. Scuseria, M. A. Robb, J. R. Cheeseman, G. Scalmani, V. Barone, B. Mennucci, G. A. Petersson, H. Nakatsuji, M. Caricato, X. Li, H. P. Hratchian, A. F. Izmaylov, J. Bloino, G. Zheng, J. L. Sonnenberg, M. Hada, M. Ehara, K. Toyota, R. Fukuda, J. Hasegawa, M. Ishida, T. Nakajima, Y. Honda, O. Kitao, H. Nakai, T. Vreven, J. A. Montgomery, Jr., J. E. Peralta, F. Ogliaro, M. Bearpark, J. J. Heyd, E. Brothers, K. N. Kudin, V. N. Staroverov, R. Kobayashi, J. Normand, K. Raghavachari, A. Rendell, J. C. Burant, S. S. Iyengar, J. Tomasi, M. Cossi, N. Rega, J. M. Millam, M. Klene, J. E. Knox, J. B. Cross, V. Bakken, C. Adamo, J. Jaramillo, R. Gomperts, R. E. Stratmann, O. Yazyev, A. J. Austin, R. Cammi, C. Pomelli, J. W. Ochterski, R. L. Martin, K. Morokuma, V. G. Zakrzewski, G. A. Voth, P. Salvador, J. J. Dannenberg, S. Dapprich, A. D. Daniels, Ö. Farkas, J. B. Foresman, J. V. Ortiz, J. Cioslowski, and D. J. Fox, Gaussian, Inc., Wallingford CT, 2009.

(5) A. D. Becke, *J. Chem. Phys.* 1993, **98**, 5648.

(6) P. L. Hay, W. R. Wadt, *J. Chem. Phys.* 1985, **82**, 270.

(7) P. C. Hariharan, J. A. Pople, *Theor. Chim. Acta* 1973, **28**, 213.

(8) R. Dennington, T. Keith, J. Millam, *Semichem Inc*., Shawnee Mission KS, 2009.

(9) T. Vogt, C. Faulmann, R. Soules, P. Lecante, A. Mosset, P. Castan, P. Cassoux, J. Galy, *J. Am. Chem. Soc.* 1988, **110**, 1833.

(10) (a) M. Yankowitz, J. Xue, D. Cormode, J. D. Sanchez-Yamagishi, K. Watanabe, T. Taniguchi, P. Jarillo-Herrero, P. Jacquod, B. J. LeRoy, *Nat. Phys.* 2012, **8**, 382. (b) I. Amidror, in *The Theory of the Moiré*

Phenomenon, ed. M. Viergever, Springer-Verlag: London, 2nd edn., 1999, vol. 1.

(11) I. Langmuir, V. J. Schaefer, *J. Am. Chem. Soc.* 1938, **60**, 1351.

(12) T. Kambe, R. Sakamoto, K. Hoshiko, K. Takada, M. Miyachi, J.-H. Ryu, S. Sasaki, J. Kim, K. Nakazato, M. Takata, and H. Nishihara, *J. Am. Chem. Soc.*, 2013, **135**, 2462.